Dynamic response of Earth's magnetosphere to B_y reversals

K. Kabin, R. Rankin, and R. Marchand
Department of Physics, University of Alberta, Edmonton, Canada

T. I. Gombosi, C. R. Clauer, A. J. Ridley, V. O. Papitashvili, and D. L. DeZeeuw
Space Physics Research Laboratory, University of Michigan, Ann Arbor, Michigan, USA

Received 10 May 2002; revised 15 November 2002; accepted 23 December 2002; published 22 March 2003.

[1] In this paper we use a three-dimensional magnetohydrodynamic (MHD) model to study the response of the magnetosphere-ionosphere system to a sudden change in the sign of the B_y component of the interplanetary magnetic field. We find that after such a change the magnetosphere responds as a linear system and the ionospheric potential can be very accurately represented by a linear superposition of the initial and final distributions of the ionospheric potential. Although heuristic in nature, this representation of ionospheric potentials significantly simplifies the analysis of the time-dependent output of the model. The accuracy of this decomposition of the ionospheric potential is discussed. This decomposition also helps to define, in a very intuitively clear way, the bow shock to ionosphere communication time and the ionospheric reconfiguration time. We find that in our model simulation the reconfiguration time depends on the strength of the interplanetary magnetic field (IMF) and the solar wind speed but not on the ionospheric conductivities. The communication time in our model has a typical value of 300–400 s and the reconfiguration time is approximately 300–450 s. These characteristic times are generally consistent with observations and earlier modeling results. *INDEX TERMS:* 2736 Magnetospheric Physics: Magnetosphere/ionosphere interactions; 2760 Magnetospheric Physics: Plasma convection; 2431 Ionosphere: Ionosphere/magnetosphere interactions (2736); 2435 Ionosphere: Ionospheric disturbances; *KEYWORDS:* Earth's magnetosphere, global MHD modeling, IMF B_y reversal

Citation: Kabin, K., R. Rankin, R. Marchand, T. I. Gombosi, C. R. Clauer, A. J. Ridley, V. O. Papitashvili, and D. L. DeZeeuw, Dynamic response of Earth's magnetosphere to B_y reversals, *J. Geophys. Res.*, *108*(A3), 1132, doi:10.1029/2002JA009480, 2003.

1. Introduction

[2] There are numerous empirical models of ionospheric convection patterns for high latitudes. Most of these models use the instantaneous values of the IMF and solar wind parameters as an input. Currently, the most commonly used models of this type are *Papitashvili et al.* [1994], *Weimer* [1995, 1996, 2001], *Ruohoniemi and Greenwald* [1996], and *Ridley et al.* [2000]. However, it is clear that the coupled system of ionosphere and magnetosphere depends not only on the instantaneous values of the solar wind parameters but also on the history of how these parameters were changing over some period of time [e.g., *Rostoker et al.*, 1988]. The description of a magnetosphere-ionosphere response to a change in the solar wind and IMF conditions is still a subject of an active research. A statistical study using the largest number of events reported to date was conducted by *Ridley et al.* [1998], who have analyzed 65 ionospheric convection changes associated with corresponding IMF changes. It has been found that in some cases the ionospheric parameters change linearly in time after the change in the solar wind. In other cases the change may be better described as an asymptotic approach to the new steady-state. *Ridley et al.* [1998] found that about 62% of the changes were linear in time, while 11% were better described by an exponential law.

[3] The time it takes the ionosphere to begin to respond to a change in the solar wind conditions has been studied for more than a decade using a variety of ground-based and spacecraft instruments and techniques [e.g., *Friis-Christensen et al.*, 1985; *Clauer and Friis-Christensen*, 1988; *Hairston and Heelis*, 1995; *Ridley and Clauer*, 1996; *Ridley et al.*, 1998; *Dudeney et al.*, 1998; *Khan and Cowley*, 1999; *Murr and Hughes*, 2001]. Although there are significant variations in the data, it may be considered established that there is a delay of 6–14 min between the moment the disturbance hits the bow shock and the moment the ionosphere starts to respond (3–11 min for magnetopause to ionosphere), and it takes another 10–30 min for the magnetosphere to completely reconfigure (excluding substorms). However, the estimations for magnetopause to ionosphere communication times during particular events vary from 3 min [*Clauer and Friis-Christensen*, 1988] to about 20 min [*Bargatze et al.*, 1985]. There is also lack of agreement between different studies if the reconfiguration time depends on the type of the IMF change, for example, whether the ionosphere reconfiguration time after a change from northward to southward IMF is the same as for a change from southward to northward [*Hairston and Heelis*, 1995; *Ridley et al.*, 1998].

0148-0227/03/2002JA009480

[4] Two scenarios have been proposed to describe the response of the ionosphere to a sudden change in the IMF. Some authors argue that there is a considerable delay in the response of the nightside of the ionosphere as compared with the dayside [*Todd et al.*, 1988; *Saunders et al.*, 1992; *Khan and Cowley*, 1999]. Other authors claim that the whole ionosphere responds essentially instantaneously to the magnetospheric disturbance [*Ridley et al.*, 1998; *Ruohoniemi and Greenwald*, 1998; *Murr and Hughes*, 2001; *Ruohoniemi et al.*, 2002]. There are also concerns about the interpretation of the data [*Lockwood and Cowley*, 1999; *Ridley et al.*, 1999; *Murr and Hughes*, 2001; *Ruohoniemi et al.*, 2002]. Thus from an observational point of view, this important question is not yet solved.

[5] Several time-accurate numerical simulations of Earth's magnetosphere provide estimations for the communication times. For example, in the model of *Slinker et al.* [1999] the ionosphere started to respond to a density pulse in the solar wind 2 min after the disturbance hit the bow shock. The same model obtained a bow shock to ionosphere communication time of 8 min for a simulation of a southward turning of the IMF [*Slinker et al.*, 2001]. In both simulations, *Slinker et al.* [1999, 2001] found that the dayside ionosphere started to respond earlier than the nightside; however the delay for the convection changes to be propagated to the nightside was quite small, on the order of 1–2 min.

[6] *Maynard et al.* [2001] performed a numerical simulation using an MHD model to analyze the dynamic response of the magnetosphere and the ionosphere to a sudden change in the IMF direction. The specific IMF change they considered was an abrupt change of the sign of B_y, which is one of the simplest possible external disturbances. They estimated the bow shock to ionosphere communication time to be about 7–8 min for the field-aligned currents. The ionospheric potential in their model started to change 4 min after the first change in the field-aligned currents. The ionosphere in their simulation responded linearly, and the ionospheric reconfiguration was completed in approximately 20 min. They also found that the whole ionosphere started to react to the B_y flip nearly simultaneously, within 1 to 2 min. The frequency of their output being 1 min, this time-scale only provided the upper bound for the time delay between the noon and the midnight. They found, however, that it takes a little longer for the nightside than the dayside to complete the transition. These findings agree with the results of the data analysis by *Dudeney et al.* [1998]. The simulation of *Maynard et al.* [2001] also indicated that the field-aligned currents reached the new steady state about 5 min before the ionospheric potential.

[7] In this study we also analyze the dynamic response of the coupled ionosphere-magnetosphere model to a flip in the B_y component of the IMF. Similar to *Maynard et al.* [2001], we choose this particular type of IMF change because it initiates probably the simplest type of ionosphere reaction. Specifically, we do not expect any substorms in the system, significant changes of the cross-polar cap potential, or other kind of violent transient reactions. We use a numerical framework similar to that of *Maynard et al.* [2001] and extend some of their results to different values of IMF and solar wind parameters. However, while *Maynard et al.* [2001] presented a very detailed analysis of a single event, we performed a large number of time-dependent calculations for a variety of solar wind conditions.

[8] The purpose of this paper is twofold. First, we find that the time-dependent ionospheric potential can be accurately represented as a linear combination of its initial and final distribution. Although this is a purely heuristic observation, it tremendously simplifies the analysis of the time dependent change of the ionospheric potentials. We emphasize that a similar decomposition may be used to study the output of other models or be applied to data analysis. Second, we study the dependency of the characteristic ionosphere reconfiguration times on the solar wind parameters and IMF strength. We also observe some differences between our results and those of *Maynard et al.* [2001] which are discussed below.

2. Model Description

[9] We use a recently developed model which describes the coupled magnetosphere-ionosphere system. The mathematical basis for the description of the magnetosphere is provided by the equations of ideal single-fluid magnetohydrodynamics. These equations are solved on a three-dimensional unstructured adaptive grid using an efficient Godunov-type finite volume method. The numerical details of this code are described by *Powell et al.* [1999], *DeZeeuw et al.* [2000], and references therein. The ionosphere is treated as a spherical conducting layer, as described below. We did not include the effects of the Earth rotation in our model. Some physical results of the application of our three-dimensional MHD model with a two-dimensional ionosphere to steady-state solar wind conditions and comparisons with the data and other magnetospheric models are described, for example, by *Song et al.* [1999, 2001] and *Gombosi et al.* [2000a, 2000b]. Also, recently a number of magnetospheric simulation have been performed to determine how closely the model compares to ground-based [*Ridley et al.*, 2001] and satellite-based [*Ridley et al.*, 2002] data.

[10] In the simulations presented in this paper we have used the technique described by *Gombosi et al.* [2002] to ensure that the Alfvén speed in the model does not exceed the speed of light but did not artificially reduce the speed of light to accelerate the calculations.

[11] The coordinate system used in the model is GSM: the X axis points from the Earth to the Sun, the Z axis is positive to the north and is in the plane which contains the X axis and Earth's dipole, and the Y axis completes the right-hand system.

[12] The ionosphere is represented by a two-dimensional layer with prescribed finite Pederson and Hall conductivities. The magnetosphere-ionosphere coupling is performed as follows [*Goodman*, 1995; *Amm*, 1996; A. J. Ridley et al., Ionospheric control of the magnetospheric configuration (1): Conductance, submitted to *Journal of Geophysical Research*, 2003a, hereinafter referred to as Ridley et al., submitted manuscript, 2003a; A. J. Ridley et al., Ionospheric control of the magnetospheric configuration: Neutral winds, submitted to *Journal of Geophysical Research*, 2003b]. Field-aligned currents are calculated within the magnetospheric module at 4 Earth radii from the center of

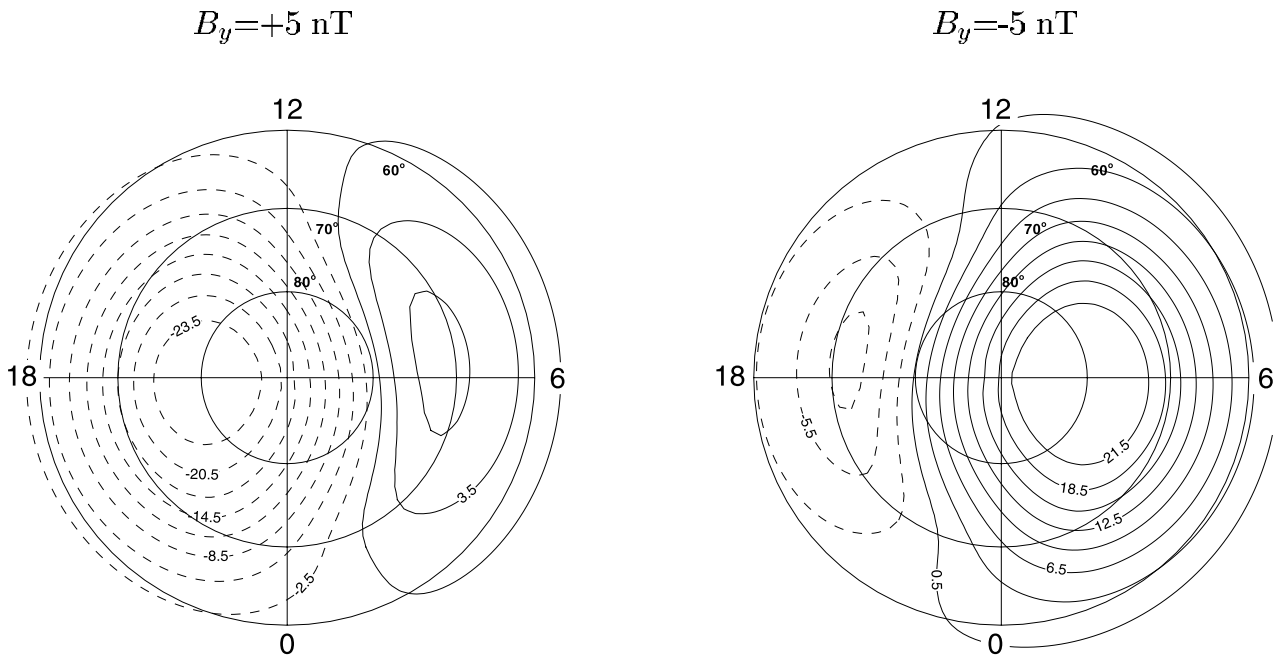

Figure 1. Initial (left panel) and final (right panel) distributions of the ionospheric potential for the baseline run. Dashed lines represent negative values of the potential.

the planet. Then these currents are mapped into the ionosphere where they are used as a source term for the two-dimensional Poisson equation for the electric potential

$$\nabla \cdot (\Sigma \cdot \nabla \phi) = -J(\lambda, \theta). \quad (1)$$

Here ϕ is the electric potential, $J(\lambda, \theta)$ is the field-aligned current which depends on the latitude λ and longitude θ, and Σ is a skew-symmetric tensor of height-integrated conductivity which describes Pederson, σ_P, and Hall, σ_H, conductivities of the ionosphere

$$\Sigma = \begin{pmatrix} \sigma_p & \sigma_H \\ -\sigma_H & \sigma_p \end{pmatrix}.$$

Once equation (1) is solved, the electric potential is mapped back to 3 Earth radii under the assumption that the magnetic field lines are equipotentials. There the convection velocity is calculated as

$$\mathbf{u} = \frac{\mathbf{B} \times \nabla \phi}{B^2}.$$

This convection velocity is used in the magnetosphere module as an inner boundary condition at 3 Earth radii. This coupling procedure is performed in the code every 5 s of real time.

[13] This approach to magnetosphere-ionosphere coupling is similar to *Slinker et al.* [2001] and *Tanaka* [2001] and somewhat simpler than that implemented in the model of *Maynard et al.* [2001] which resolves the vertical structure of the ionosphere. The two-dimensional ionosphere, however, is usually quite adequate for a study of the solar wind effects on the ionospheric convection.

[14] One limitation of the magnetosphere-ionosphere coupling being performed in this manner is that the field-aligned currents (whether caused by Alfvén waves or global reconfigurations) which reach 4 R_E are instantly transmitted to the ionosphere. This can cause problems with estimates of time delays, although these are minor, since the time it takes an Alfvén wave to propagate from 4 R_E to 1 R_E is quite small. Another, possibly more significant issue is that Alfvén waves which reach 4 R_E do not have a chance to be reflected back towards the magnetosphere from the outer wall of the ionospheric cavity between 4 R_E and 1 R_E. Therefore in reality the ionosphere sometimes does not react to those Alfvén waves, while in our simulation it does. The simulation performed by *Maynard et al.* [2001] does not have this problem, since they simulate the magnetosphere-ionosphere system as a whole, instead of having a null zone, such as exists in our simulations between 3 R_E and 1 R_E. This issue will be further addressed in the discussion section below.

[15] We output the results of the model calculation every 20 s, as compared with 1 min by *Maynard et al.* [2001]. This is a minor improvement which gives us a slightly higher time resolution than that displayed by *Maynard et al.* [2001].

3. Initial Conditions

[16] Steady-state ionospheric convection patterns for the IMF conditions dominated by a B_y component are well-known and consist of a "banana" and "orange" convection cells [e.g., *Cowley*, 1981]. Figure 1, left panel shows the steady state solution for the ionosphere electric potential achieved in our model for the following solar wind parameters: solar wind density 5 cm^{-3}, solar wind velocity 500 km/s, solar wind temperature 15.6 eV, magnetic field B = (0, 5, 0) nT. The right panel of Figure 1 shows the steady state solution for the same solar wind parameters, except that B_y is negative: B = (0, −5, 0) nT. For reference, Figure 2 shows

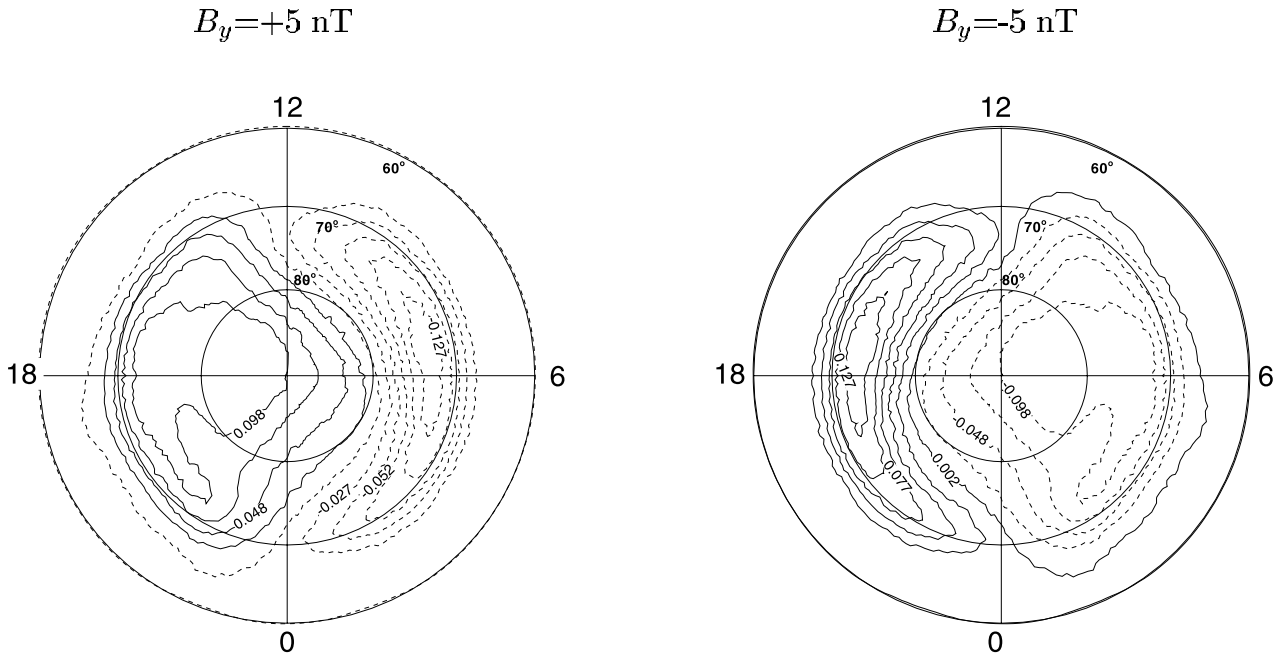

Figure 2. Initial (left panel) and final (right panel) distributions of the field aligned currents. Dashed contours represent the currents into the ionosphere and solid contours currents away from ionosphere. Note that our model does not reproduce region 2 currents.

the field-aligned currents entering and leaving ionosphere in these two steady states. Note that the region 2 currents are not reproduced in single-fluid MHD models, such as ours. To obtain region 2 currents requires that the MHD code be coupled to a multifluid inner magnetosphere model, such as the Rice Convection Model, which can address the gradient and curvature drifts of the inner magnetospheric plasma. The ionospheric conductivities for these simulations were chosen to be uniform with height integrated Pederson conductivity being 5 S and Hall conductivity 10 S. Earth's dipole moment was assumed to be along the Z axis and have a value of -7.9×10^{15} T m^3. The parameters chosen for this simulation are fairly typical for the Earth environment. However, in order to facilitate analysis and make the results more clear, somewhat idealized conditions were studied. In particular, the ionospheric conductivity was assumed to be uniform and Earth's dipole was not tilted. We consider a simulation with this set of parameters to be our "baseline" run. As discussed later in the text we have also performed a number of simulations with different IMF intensities and solar wind velocities.

[17] It is expected, if there is no significant hysteresis in the system, that the ionospheric steady states for B_y positive and B_y negative are just mirror images of each other. This assumption was carefully tested and found to be true for an MHD model by *Tanaka* [2001], at least for uniform ionospheric conductivities. For our model, indeed, one can see from Figures 1 and 2 that if $J_0(\lambda, \theta)$ is the steady-state distribution of the field-aligned currents in the ionosphere for B_y = +5 nT, then $-J_0(\lambda, \pi - \theta)$ is the steady-state distribution of the currents for $B_y = -5$ nT. Naturally, by virtue of equation (1), exactly the same relation holds for the distribution of the electric potential in the ionosphere. That is, if $\phi_0(\lambda, \theta)$ is the steady-state distribution of the potential corresponding to B_y = +5 nT, then $-\phi_0(\lambda, \pi - \theta)$ is the potential for $B_y = -5$ nT. We note that many empirical ionospheric models show a certain degree of asymmetry between the solar wind conditions which differ only in the sign of B_y. These effects are attributable to a nonuniform Hall conductance in the ionosphere, which causes a significant asymmetry between the dawn and dusk cells (Ridley et al., submitted manuscript, 2003a).

[18] In this paper we study the reaction of magnetosphere-ionosphere system to a sudden change of the sign of the IMF B_y. For simplicity, we assume that B_y is the only component of the IMF. This is a very special type of MHD discontinuity which is simultaneously a rotational and tangential discontinuity [*Landau and Lifshitz*, 1984]. It is a current sheet in the solar wind with the currents directed along the Z axis and the linear current density being $B_y c/2\pi$. In the uniform plasma flow upstream of the bow shock this current sheet remains flat and propagates at the plasma speed (because there is no magnetic field component perpendicular to the surface of the discontinuity). However, the plasma flow becomes nonuniform behind the bow shock in the magnetosheath. As a result, the B_y discontinuity sheet bends and its propagation speed starts to depend not only on the plasma velocity but on the Alfvén and sound velocities as well. The closer the disturbance gets to Earth the more dominant the contribution of the Alfvén speed to the propagation speed becomes. In fact, the current sheet associated with B_y sign flip loses its identity in nonuniform plasma flow in the magnetosheath and becomes a more general and complicated type of disturbance.

[19] After the initial steady-state was computed for a positive B_y we modified these initial conditions by changing the sign of B_y in the cells with $X > R_{BS}$, where R_{BS} is the subsolar stand-off distance of the bow shock. This allows us to avoid much of the smearing of the current sheet that arises due to numerical resistivity and viscosity as well as

save some computational time, since we do not need to convect the B_y discontinuity from the upstream boundary at $X = 32\ R_E$. Of course, after the first few time-steps, numerical resistivity and viscosity spread the B_y discontinuity over 2–3 cell sizes. The cell size in this area of the simulation was 0.25 R_E which leads to the initial thickness of the current sheet of about 0.5 R_E as compared to about 4 R_E in the simulation of *Maynard et al.* [2001].

4. A Simple Approximation for the Ionospheric Potential

[20] In the steady state at Earth the IMF B_y component interaction with the dipole field produces merging sites at the Northern Hemisphere duskside and Southern Hemisphere dawnside for $B_y > 0$. The locations of the merging sites are reversed for $B_y < 0$. Eventually, after an abrupt change of the sign of B_y, the magnetosphere-ionosphere system reaches a new steady state. As described in section 3, we expect the new steady-state to be a mirror image of the initial steady-state. In this paper we concentrate on the path the ionosphere takes to evolve from the initial state governed by solar wind B_y positive to the final state governed by B_y negative.

[21] One of the purposes of this paper is to find a simple way to represent the time-dependent evolution of the ionospheric potential after the B_y flip. The natural way to do so is to expand the ionospheric potential pattern in terms of prescribed base functions. Obviously, the initial and final ionospheric patterns need to be reproduced; therefore they constitute the absolute minimum of the basis. If needed, other functions can be added to the basis. An expansion of this type is, of course, just a heuristic assumption whose justification is provided only by the small error of the final approximation. In this work we show that the simplest possible one-parameter expansion works reasonably well for this problem.

[22] Bearing the above in mind, we suggest to represent the ionospheric potential and field-aligned currents during the evolution after the flip of the B_y component of the magnetic field as

$$J(\lambda,\theta,t) = J_0(\lambda,\theta)a(t) - J_0(\lambda,\pi-\theta)(1-a(t)). \qquad (2)$$

Similarly, the ionospheric potential is represented as

$$\phi(\lambda,\theta,t) = \phi_0(\lambda,\theta)a(t) - \phi_0(\lambda,\pi-\theta)(1-a(t)). \qquad (3)$$

[23] Here $J_0(\lambda, \theta)$ and $\phi_0(\lambda, \theta)$ are the steady-state initial (before the B_y change occurred) distributions of the field-aligned currents and the ionospheric potential respectively, and $a(t)$ is a single adjustable coefficient in the scheme which is determined at each time by minimizing the mean-square difference between the ionospheric potential (or field-aligned currents, which gives an almost identical result) calculated in the model at time t and approximation (2) or (3). As explained in section 3, $-\phi_0(\lambda, \pi - \theta)$ and $-J_0(\lambda, \pi - \theta)$ are the distributions of the ionospheric potential and field-aligned currents at $t \to \infty$.

[24] Figure 3 demonstrates the relative error of the expansions (2) or (3). Lines 1 and 2 represent the mean-square error for the potential and the field-aligned currents

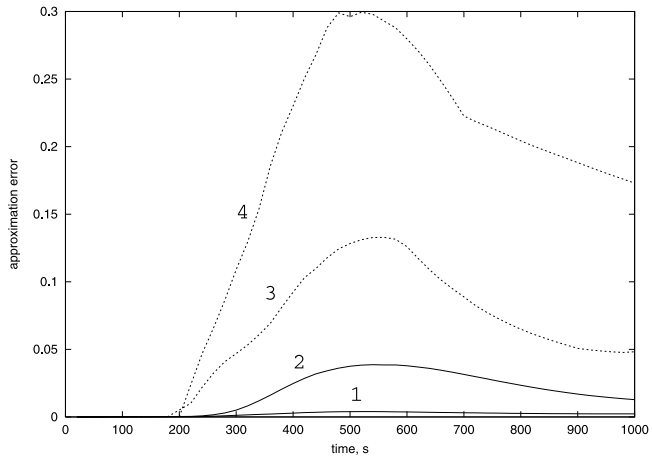

Figure 3. The errors in representing the potential and field-aligned currents as a linear superposition of the initial and final states. Line 1 shows the mean-square error in the potential, line 2 shows the mean-square error in the field-aligned currents, line 3 shows the pointwise error in the ionospheric potential, and line 4 shows the pointwise error in the field-aligned currents. All the errors are computed for our "baseline" simulation with initial $B_y = 5$ nT.

respectively. This definition of error is based on a discrete equivalent of the L_2 (mean-square) norm:

$$\|\,\mathrm{error}(t)\|_2 = \frac{\sum_{\lambda,\theta}\left(\phi^{MHD}(\lambda,\theta,t) - \phi(\lambda,\theta,t)\right)^2}{\sum_{\lambda,\theta}\left(\phi^{MHD}(\lambda,\theta,t)\right)^2}. \qquad (4)$$

Here ϕ^{MHD} is the ionospheric potential calculated in the MHD model at time t and ϕ is the ionospheric potential approximated with the formula (3). The summation extends over the whole high-latitude area (above 50° latitude in our simulation). One can see that expansions (2) or (3) are very accurate in the mean-square sense, the relative error is about 4% for field-aligned currents and about 0.4% for the ionospheric potential. It is not surprising that the error for the field-aligned current is larger than for the potential. The field-aligned currents in an MHD code are computed from $\nabla \times \mathbf{B}$ which involves numerical differentiation. Numerical differentiation is an intrinsically imprecise procedure, and as a result, the currents are usually fairly noisy. In contrast, the ionospheric potential is computed by solving an elliptic Poisson equation whose solutions are always smooth, even if the right-hand side of the equation is not. As a result, numerical errors in computing the currents translate into larger L_2 distances between the field-aligned currents at two different times. The contrast between smooth potentials and noisy currents is clearly seen in Figures 1 and 2.

[25] Although mean-square norm is used very commonly, it provides only some kind of global estimation of precision: while the total error may be quite small, there still can be local regions with large differences. A more demanding measure of accuracy is a pointwise (L_∞) error which is defined as the maximum of the absolute value of the difference of the two functions:

$$\|\mathrm{error}(t)\|_\infty = \frac{\max_{\lambda,\theta}\left|\phi^{MHD}(\lambda,\theta,t) - \phi(\lambda,\theta,t)\right|}{\max_{\lambda,\theta}\left|\phi^{MHD}(\lambda,\theta,t)\right|}.$$

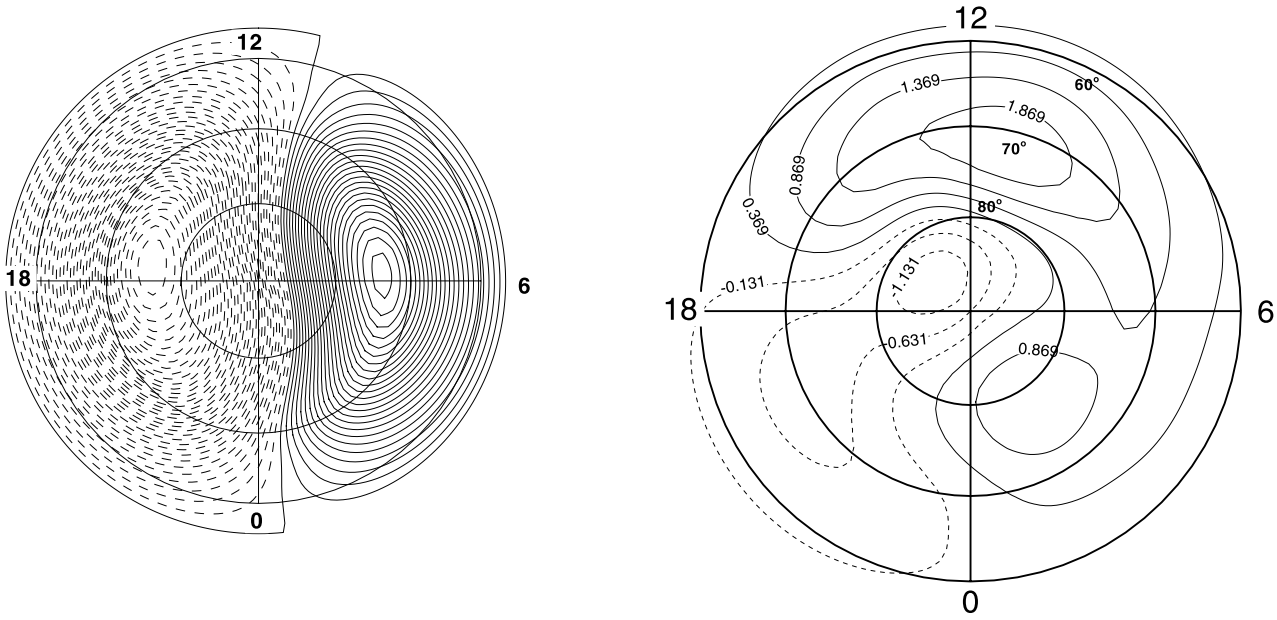

Figure 4. (left) The calculated in the MHD model potential distribution pattern at t = 530 s. (right) The error distribution at this time; that is the difference between the computed MHD potential and the approximation given by equation (3). Contour lines on both plots are separated by 0.5 kV.

The notations here are the same as in equation (4). The dashed line 3 and 4 in Figure 3 show the error using this norm for the ionospheric potential and the field-aligned currents respectively. This kind of error is significantly larger than the mean-square one, but still it is only about 10% for the ionospheric potential and 30% for the field-aligned currents at the maximum. Note that everywhere in this paper we have calculated the coefficient $a(t)$ by minimizing only the mean-square norm of the error. No attempt to improve accuracy in L_∞ sense has been made. Considering the uncertainties of MHD models we feel that this level of accuracy is quite acceptable for such a simple approximation.

[26] Figure 4 shows the ionospheric potential computed in the MHD model, $\phi^{MHD}(\lambda, \theta, t)$, and the distribution of the error of equation (3), $\phi^{MHD}(\lambda, \theta, t) - \phi(\lambda, \theta, t)$, at time t = 530 s. This time corresponds to the peak on the approximation error. The contours on the plot are separated by 0.5 kV. The potential drop across the polar cap is 33.5 kV but it is only 3.5 kV across the potential difference pattern. This gives about the same magnitude for the error in the ionospheric potential as the pointwise norm: about 10%. These considerations of the error in several different representations provide the justification for using formulas (2) or (3). While we feel that these formulas are useful for the study of magnetosphere-ionosphere timing and ionospheric response for this particular type of IMF change, one should keep in mind that this representation is intrinsically approximate in nature and may not be applicable to every possible IMF change.

[27] Representation (3) is similar to the residual patterns technique used by *Ridley et al.* [1998] and *Maynard et al.* [2001], but has a much stronger message: we suggest a way to describe what the residual pattern is and how it evolves with time. Equation (3) not only tells us the manner in which some characteristic number, such as the maximum cross polar cap potential difference, changes with time but quantifies the manner in which the whole two-dimensional potential pattern evolves. Effectively, we reduce a three-dimensional (3-D) function to a product of a 2-D function and 1-D function, which drastically reduces the amount of information to be analyzed. It is interesting that discussing potential difference patterns, *Maynard et al.* [2001, p. 21,437] mentions that "the center of the pattern remains constant and grows in magnitude..." which implies that decomposition (3) will most likely work well for the results of their calculation. Indeed, Plates 2 and 7 of *Maynard et al.* [2001] which show the difference patterns for the ionospheric potential and field-aligned currents exhibit little topological change with time; only the magnitude of the difference increases in time.

[28] For the purpose of comparison with the earlier publications which utilized residual patterns, we show in Figure 5 (left panel) the residual pattern for the ionospheric potential defined with respect to a fixed initial distribution: $\phi^{RES}(\lambda, \theta) = \phi(\lambda, \theta, t) - \phi(\lambda, \theta, t_0)$ for the time corresponding to the maximum error, t = 530 s and t_0 = 0. The right panel of Figure 5 shows $\phi_0(\lambda, \theta) + \phi_0(\lambda, \pi - \theta)$, which is a time-independent residual pattern in expansion (3). This pattern only scales with time (hence, there is no contour labels in this figure). The two potential residual patterns shown in Figure 5 are quite similar. They both fit the description of type 1 patterns of *Ridley et al.* [1998]: "a single positive or negative cell centered on the noon meridian." *Ridley et al.* [1998] found this type of residual pattern typical for B_y changes, although they considered cases with significant B_z. The actual residual pattern in the MHD model is, however, less symmetric than the idealized one suggested by equation (3), which is also demonstrated by the asymmetric distribution of the error in Figure 4.

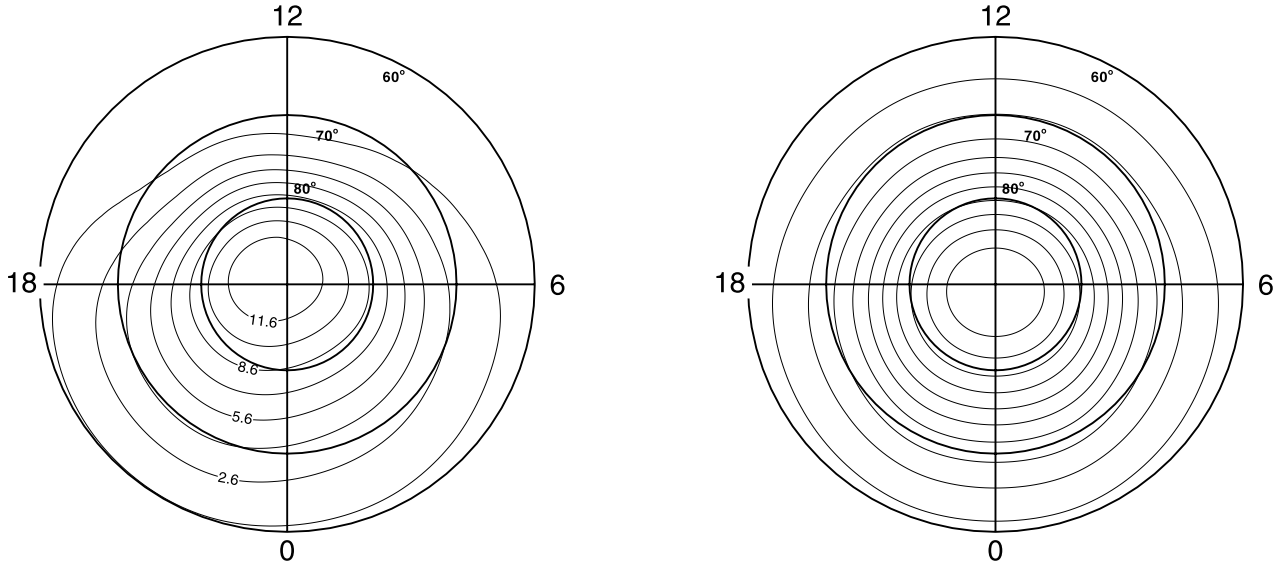

Figure 5. Difference pattern in the ionospheric potential at time t = 530 s (left panel) and the residual pattern in approximation (3) (right panel).

[29] For completeness, Figure 6 shows the corresponding residual patterns for the field-aligned currents for the same moment in time, 530 s. As suggested by a larger error in the field-aligned currents, the asymmetry of the MHD residual pattern for the currents is even larger than that for the ionospheric potential. Both patterns in Figure 6 are similar in a sense that they represent a cell of positive (out of ionosphere) currents elongated in the dawn-dusk direction centered close to the magnetic pole surrounded by a belt of negative currents.

[30] Our Figures 5 and 6 should be directly compared to Plates 2 and 7 of *Maynard et al.* [2001]. It is easy to see that their difference patterns also do not change significantly in time, which means that most likely, their simulation results may be well approximated by a formula similar to equation (3). There are some differences between the two models, though. The potential difference pattern in the simulation of *Maynard et al.* [2001] is more stretched out into the nightside and has a small cell of negative potential on the dayside, which is absent in our simulation. The field-aligned currents difference pattern in the model of *Maynard et al.* [2001] shows a concentrated cell of currents into the ionosphere on the dayside, while our simulation shows negative current region distributed more evenly around the central region of positive currents. We believe that the differences between the two models may be attributed to the different conductance distributions and the different approaches to the magnetosphere-ionosphere coupling.

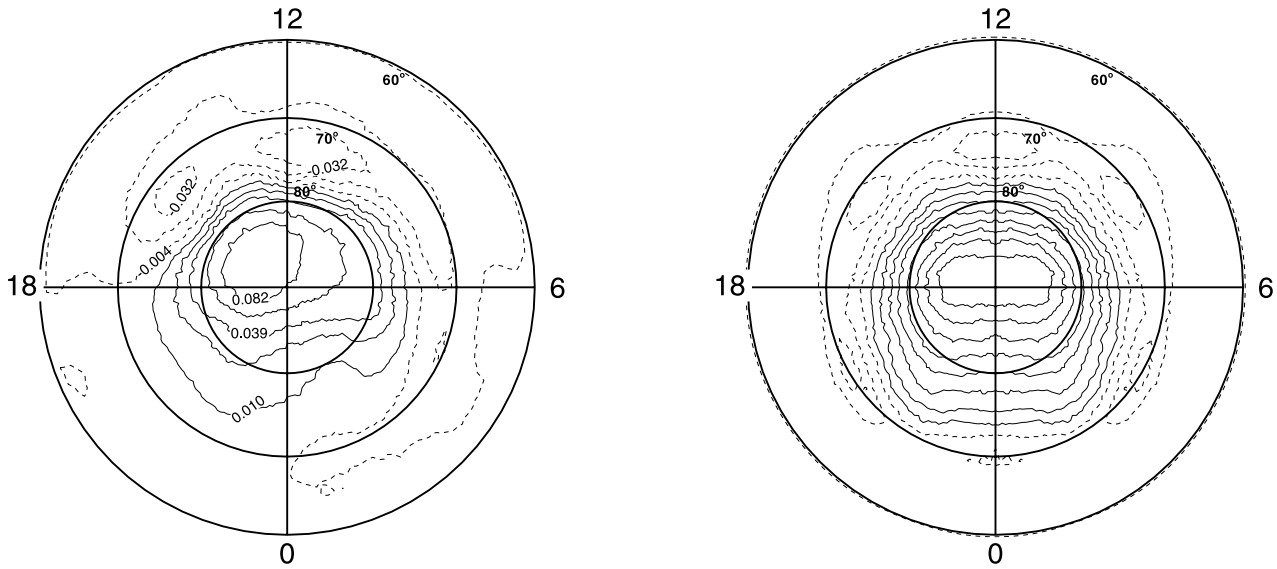

Figure 6. Difference pattern in the field aligned currents at time t = 530 s (left panel) and the residual pattern in approximation (2) (right panel).

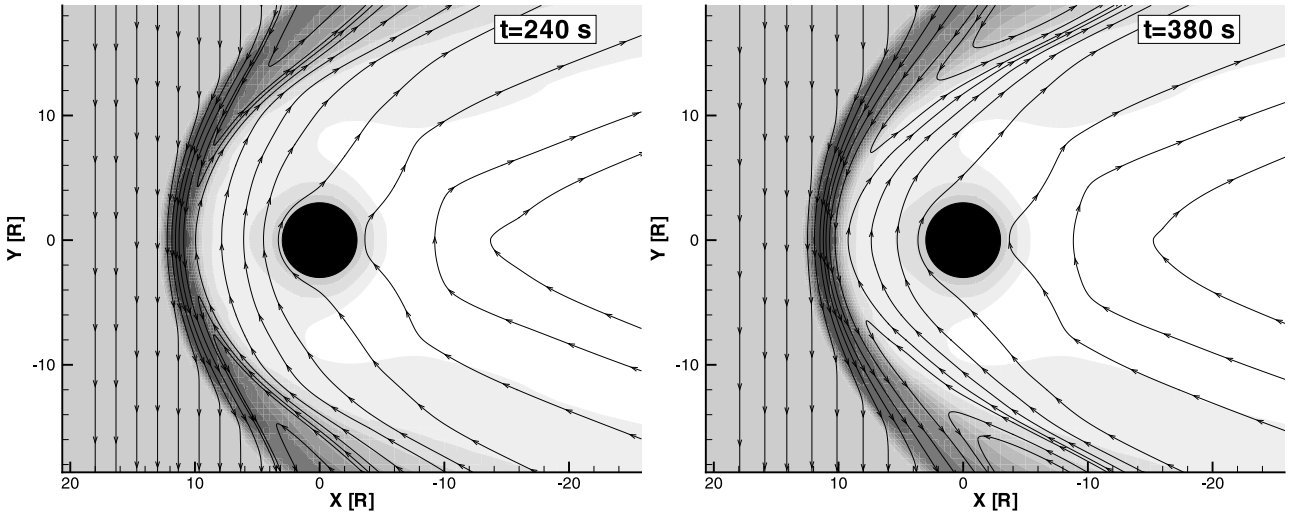

Figure 7. Magnetic field lines in the equatorial plane of the simulation at time t = 240 s and 380 s. The grey scale is density, which helps to identify the bow shock and the magnetopause.

[31] It has been understood for a long time that that magnetosphere-ionosphere system has a memory of its previous condition [e.g., *Rostoker et al.*, 1988]. We believe that our results should be of use to the future generation of empirical ionospheric models which incorporate not only current solar wind conditions but also a convolution of the IMF conditions over a certain preceding period. A first approach to such an ionospheric model is described by *Valdivia et al.* [1999]. In a different work devoted to essentially the same problem, *Ridley et al.* [2000] used a linear combination of potential patterns, similar to equation (3), for predicting the future ionospheric potential pattern, given a nowcast and upstream IMF conditions.

5. Dynamics of B_y Reversal in the Magnetosheath and Ionospheric Response

[32] Figure 7 shows the magnetic field lines and plasma density in the equatorial plane of our simulation for two different times, 240 s and 380 s after the B_y discontinuity has encountered the bow shock. Note that Figure 7 shows the field-lines plotted using only the X and Y components of the magnetic field; the Z component is completely ignored in a two-dimensional plot. The plasma speed behind the bow shock is much higher in the flanks than near the subsolar line. Therefore a planar current sheet coming from the solar wind will become quite distorted in the magnetosheath. This draping is clearly seen in Figure 7 and in Plate 3 of *Maynard et al.* [2001]. Once the B_y reversal reached the magnetosheath, the magnetic reconnection with oppositely directed magnetic field in the magnetosheath begins. This is what was called IMF-IMF reconnection by *Maynard et al.* [2001]; it also can be seen in Figure 7.

[33] Time t = 240 s (4 min) shown in Figure 7 corresponds to the time when the B_y flip has reached the magnetopause and the IMF field behind it started reconnecting with the Earth's magnetic field. Once the magnetic field reversal has reached the magnetopause it stops propagating forward, and the further evolution of the magnetopause is described by the erosion due to the magnetic reconnection. This erosion is further demonstrated by a snap-shot at a later time, t = 380 s.

[34] The propagation of B_y reversal across the magnetosheath is further illustrated in Figure 8 which shows a sequence of 25 B_y profiles along the Sun-Earth line for times separated by 20 s. As described in section 3, we have initialized the simulation at t = 0 with the B_y discontinuity just upstream of the bow shock (at X = 13 R_E for this run). As a result of our initialization procedure, we start the simulation with a sharper discontinuity than *Maynard et al.* [2001] (0.5 R_E versus 4 R_E). This difference in the initial conditions may account for some of the differences in our results. In Figure 8 one can see the propagation of the B_y change across the magnetosheath. It is clear that the propagation speed of this current sheet associated with the B_y reversal decreases as the discontinuity approaches the magnetopause. This is consistent with the velocity profile in the magnetosheath that is presented in Figure 9.

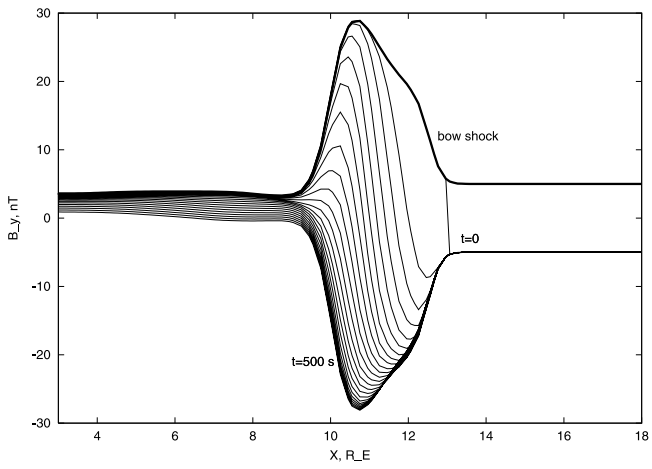

Figure 8. Propagation of the B_y flip through the magnetosheath along the Sun-Earth line. The B_y profiles are separated by 20 s intervals. The thick line shows the B_y distribution in the initial steady-state.

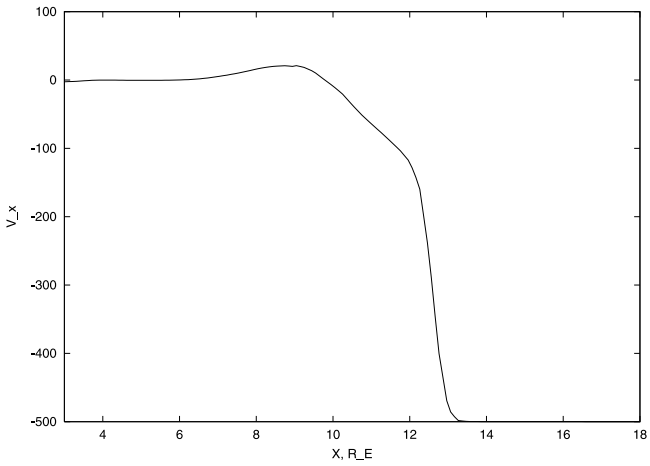

Figure 9. The plasma speed distribution in the magnetosheath along the Sun-Earth line.

This slowdown is also consistent with the slowdown observed by *Slinker et al.* [1999] for a density pulse. Once the B_y reversal enters the magnetosheath, the oppositely directed magnetic fields start to reconnect (IMF-IMF reconnection in terminology of *Maynard et al.* [2001]). This is the mechanism which gradually replaces the positive peak in B_y in the magnetosheath with the negative peak, which can be seen in Figure 8. This process also reverses the tilt of the magnetic field at the magnetopause and reconfigures the magnetopause currents [*Maynard et al.*, 2001]. The newly reconnected IMF field lines move into the flanks of the magnetosheath and thus propagate the information about the B_y reversal further downstream. The reconnection process also gives rise to magneto-acoustic and Alfvén waves which eventually communicate the information about the changes to the ionosphere.

[35] The magnetic reconnection process is responsible for the change of the magnetic field inside the magnetopause. It can be seen in Figure 8 that in the sheath, there is a clear wave-like propagation of the B_y reversal. The situation is quite different inside the magnetosphere. In our model, the B_y component inside the magnetosphere is essentially constant along the Sun-Earth line. Once the disturbance reaches the magnetopause, the wave-like motion along the X axis disappears. Instead, the B_y value inside the magnetopause gradually changes almost uniformly for $3\ R_E < X < 10\ R_E$.

[36] The fact that the error in the representation (3) is so small indicates that in our model the whole ionosphere responds to the external disturbance essentially simultaneously. This fact is further illustrated by Figure 10 which shows the change with time of the ionospheric potential at the fixed locations along the 73° parallel, separated by 2 hours of magnetic local time (MLT, or 30° in magnetic longitude). The latitude of 73° was chosen because it is usually close to the maximum and minimum of the ionospheric potential pattern. Each line in Figure 10 is labeled by the MLT it corresponds to. In Figure 10, all the points start to react to the change in IMF conditions at nearly the same time. However, at 1200, 1000, 0800, and 0600 MLT there is first a small reduction (at $t = 200 - 250$ s) of the potential followed by an asymptotic increase to the new equilibrium value. The cause of this initial reduction in the dayside potential is unclear and might be numerical. As discussed in section 6, we define $t \approx 300$ s as the beginning of the ionospheric response, at which time the large-scale reconfiguration of the ionospheric potential undoubtedly associated with the IMF reversal beings.

[37] In our study of ionospheric response to a reversal of the IMF B_y there is no noticeable wave propagation from noon to midnight, such as discussed by *Khan and Cowley* [1999]. The ionospheric potential at all locations approaches the new steady-state value exponentially rather than linearly in time, consistent with the global ionospheric potential pattern, as described in section 6. Thus, our results concerning the qualitative characteristics of the ionospheric response agree with the data analysis presented by *Ridley et al.* [1998], *Ruohoniemi and Greenwald* [1998], and *Murr and Hughes* [2001] but are in disagreement with those of *Khan and Cowley* [1999] and *Lockwood and Cowley* [1999]. The MHD simulation of *Maynard et al.* [2001] also found that the whole ionosphere starts to react to the magnetospheric disturbance at nearly the same time. However, they claim that the reconfiguration takes longer at the nightside than on the dayside and in the polar cap. The reasons contributing to a nearly simultaneous reaction of the whole ionosphere are discussed by *Ridley et al.* [1998], *Shepherd et al.* [1999], and *Maynard et al.* [2001].

6. Ionospheric Response Times

[38] Figure 11 shows the variation of the coefficient a in equations (2) and (3) with time for four different simulations. The solar wind parameters for the simulations presented in Figure 11 are solar wind density 5 cm^{-3}, solar wind speed 500 km/s, and solar wind temperature 15.6 eV. The direction of the IMF in all these simulations was reversed from the positive Y direction to the negative Y direction. Changing the sign of B_y from negative to positive will result in an identical time dependence of $a(t)$. The magnitudes of B_y are the following: open circles 10 nT,

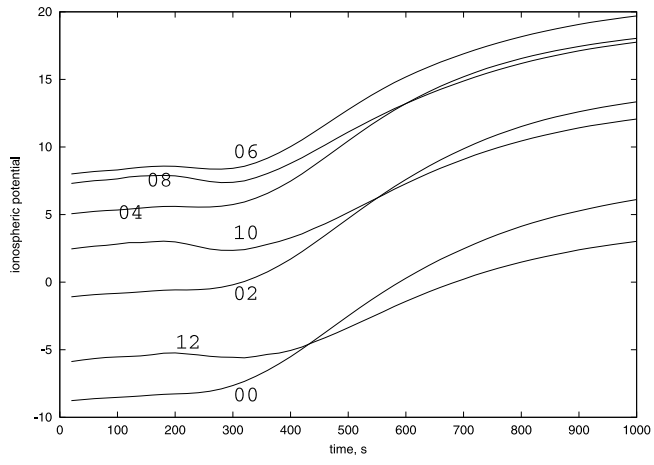

Figure 10. The time change of the ionospheric potential at seven fixed locations at 73° northern latitude. Each line is labeled by the local magnetic time it corresponds to. Our model runs have the dipole moment of Earth aligned with the Z axis of the GSM coordinate system, so there is no difference between the local time and magnetic local time.

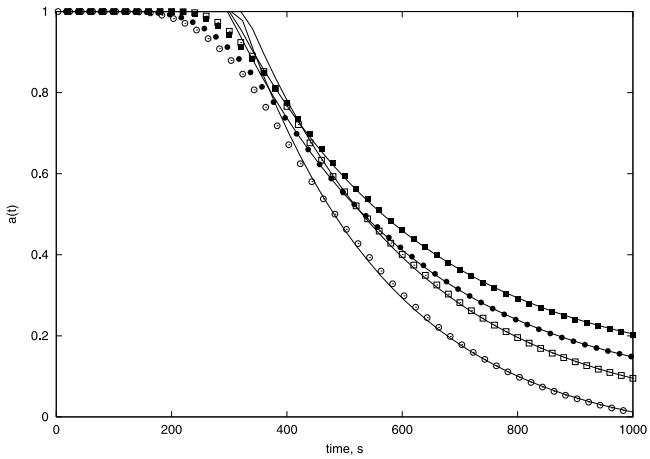

Figure 11. Time evolution of the ionospheric convection pattern. Coefficient $a(t)$ is defined by the equation (2). The solar wind parameters for these simulations are identical, except for the IMF strength. Open circles correspond to the IMF strength 10 nT, open squares 5 nT, solid circles 3 nT, and solid squares 2.5 nT. The thin solid lines show the exponential fits to the asymptotics of $a(t)$.

open squares 5 nT, solid circles 3 nT, and solid squares 2.5 nT.

[39] The time $t = 0$ in all these simulations corresponds to the moment when the B_y reversal reaches the bow shock. We note that most other studies used the moment the disturbance arrives at the magnetopause as $t = 0$. Whenever we compare our results to those of such studies we always account for this difference. We prefer our choice of the initial time because the moment a disturbance arrives at the bow shock is defined much more clearly than the moment a disturbance arrives at the magnetopause. In general, it may be difficult even to say where the disturbance encounters the magnetopause for the first time. In addition, magnetic reconnection which occurs in the magnetosheath and at the magnetopause further complicates the precise definition of the time when a disturbance arrives at the magnetopause.

[40] The time evolution of the coefficient $a(t)$ clearly consists of two distinct parts. First, for some time t_0, $a(t)$ is essentially constant in time. This period corresponds to the propagation of the discontinuity from the bow shock to the ionosphere. Once the disturbance has reached the ionosphere, $a(t)$ decays in time and this decay can be described very well by $e^{-t/\tau}$, as shown by thin continuous lines in Figure 11. Thus there are two characteristic time scales: the bow shock to ionosphere communication time, t_0 and the reconfiguration time (using the terminology of *Murr and Hughes* [2001]) which describes how fast the ionosphere relaxes to the new steady-state. We note the exponential approach of the ionosphere to the new steady-state. Exponential functions are usually associated with first order linear ordinary differential equations, which indicates that at least for simple changes of the IMF conditions the magnetosphere-ionosphere system behaves like a linear system.

[41] For all these simulations the bow shock to ionosphere communication time is essentially the same, $t_0 \approx$ 300 s, virtually independent of the IMF strength. Although there are some small local changes in the ionospheric potential as early as 200 s, these changes are too small to be observed in the variation of the coefficient $a(t)$. The lack of dependence of the bow shock to ionosphere communication time on the IMF strength is not surprising since the B_y discontinuity we are studying propagates in uniform plasma with the plasma flow speed. Although the plasma flow in the magnetosheath is nonuniform, it still has a certain degree of symmetry and it is reasonable to expect that the B_y discontinuity will still be advected essentially with the local plasma flow speed. However, unlike the communication time, the reconfiguration time depends on the IMF strength. Once again, this is expected, since the reconfiguration time will be determined by the Alfvén and magneto-acoustic waves communicating the information from the magnetopause to the ionosphere and back. The reconfiguration times we inferred from our model are summarized in Table 1.

[42] We have repeated some of the simulations described above with higher values of the Hall and Pederson conductances: σ_H = 20 S and σ_P = 10 S. However, the reconfiguration times show no dependence on the value of conductances; only the magnitude of the ionospheric potential changed. This means that the ionosphere reconfiguration in our model is controlled by the communications between the ionosphere and various parts of the magnetosphere rather than the dissipation of the plasma circulation in the ionosphere itself. To some extent, this result may be related to the absence of the region 2 currents in our model.

[43] We have also performed a series of simulations with different values of the upstream solar wind velocity: V_x = 350 km/s, 400 km/s, and 450 km/s. The temperature in this model runs was T = 40 eV, and the magnetic field was B_y = 5 nT. The calculation with V_x = 350 km/s has the same parameters as those of *Maynard et al.* [2001]. Figure 12 shows the results of these simulations compared to a simulation with the solar wind parameters considered earlier: V_x = 500 km/s, T = 15.6 eV, and B_y = 5 nT. Clearly, both the communication and reconfiguration times are longer for the simulation with the lower solar wind speed. For this simulation we obtained the communication times similar to those of *Maynard et al.* [2001] for field-aligned currents. In the simulation of *Maynard et al.* [2001] the field aligned currents in the ionospheric region begin to change about 4 min prior to the change in ionospheric potential. This delay does not appear in our model. The bow shock to ionosphere communication time in our simulation was approximately 400 s (6.7 min) as compared with 8 min obtained by *Maynard et al.* [2001] for field-aligned currents. (However, it is possible to interpret their plots in Figures 2 and 3 as suggesting some ionospheric response at about

Table 1. Reconfiguration and Bow Shock to Ionosphere Communication Times

V_x, km/s	B_y, nT	t_0, s	τ, s
500	2.5	300	322.1
500	3.0	300	314.6
500	5.0	300	297.4
500	10.	300	258.5
450	5.0	320	326.6
400	5.0	370	426.5
350	5.0	400	446.9

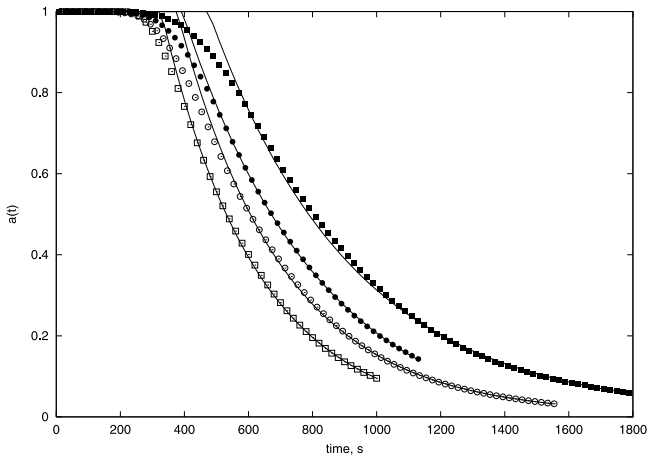

Figure 12. Time evolution of the ionospheric convection pattern. Coefficient $a(t)$ is defined by the equation (2). Open squares correspond to a simulation with the solar wind speed 500 km/s, open circles to 450 km/s, closed circles to 400 km/s, and solid squares to 350 km/s. The IMF intensity in all cases is 5 nT. The thin solid lines show the exponential fits to the asymptotics of $a(t)$.

6 min.) There are certainly enough differences in the two models to account for this difference in timing. The longer communication time for lower solar wind speeds can be clearly understood as a result of combining two following factors: first, the advection speed of the B_y flip is slower and second, because of the smaller dynamic pressure of the solar wind, the bow shock is further away from Earth: at about 15 R_E as opposed to 13 R_E.

[44] Just as in the rest of our simulations, we obtained an exponential approach in time of the ionosphere to the new steady-state, while *Maynard et al.* [2001] observed a linear change of the parameters with time. However, we feel that their Figure 2 may also be consistent with an exponential decay. Another possibility for this discrepancy is that in our computations the B_y reversal was much sharper, as explained in section 3. Nevertheless, the two MHD simulations have produced very similar reconfiguration times. In the simulation of *Maynard et al.* [2001], it took approximately 20 min of change for the ionosphere to be within 10% of the new steady state. This time is essentially the same in our simulation as well, as revealed by Figure 12. These characteristic times are also within the observational constraints, such as those inferred from the data by *Ridley et al.* [1998]: 8.4 ± 8.2 min for magnetopause to ionosphere communication time (which is approximately 12 ± 9 min for bow shock to ionosphere communication time) and 7–30 min for the ionosphere reconfiguration. As it is evidenced by the very large error bars, the spread of the estimations for the communication time in the data is quite large, and there are studies which present events with significantly smaller communication times, such as 3 min [*Clauer and Friis-Christensen*, 1988]. Thus the communication times in our model are quite reasonable as compared to the available measurements.

[45] One discrepancy between the modeling results and observations is the nighttime potential taking longer to reconfigure than the dayside potential, as was observed in the data by *Murr and Hughes* [2001] and in a simulation by *Maynard et al.* [2001]. The recent study by *Lu et al.* [2002] also shows this tendency. They explain this tendency as being caused by Alfvén waves bouncing off the conducting ionospheric, without actually causing changes in the electric potential in the ionosphere. They speculate that because the nightside conductance is so different compared to the dayside conductance, the reconfiguration times will be different. Our numerical simulation does not show this effect, but because of the instantaneous translation of Alfvén waves at 4 R_E to 1 R_E, the Alfvén wave bouncing cannot be simulated. Also, we have used only uniform ionospheric conductivities in this work.

7. Conclusions

[46] In this paper we presented results of a series of 3-D MHD simulations of the response of Earth's magnetosphere-ionosphere system to a sudden change in the B_y component of the IMF. We found that for this type of disturbance, the ionospheric electric potential can be represented as a superposition of its initial and final distributions. This decomposition drastically simplifies the analysis of the time dependent model results, and an adaptation of this model also allows a very natural definition of the bow shock to ionosphere propagation time and the ionosphere reconfiguration time. Our method of analysis also highlights the distinction between these two characteristic times. The results of our model also provide an initial step towards the development of empirical models of high latitude ionosphere convection which will include hysteresis effects. The methodology and the initial approach to this very complicated problem is given by *Valdivia et al.* [1999].

[47] In our model calculations the ionosphere responds to a change in the IMF as a single entity (there is no significant delay in response between the dayside and the nightside) and approaches the new steady state exponentially in time. Although questioned by many, a similar ionospheric behavior has been observed; see *Ruohoniemi et al.* [2002] for a recent review of this controversy. We would also like to note that both *Maynard et al.* [2001] and the current work investigated a disturbance having a front perpendicular to the solar wind speed. In reality, the plane of the discontinuity in the solar wind may be tilted with respect to the solar wind velocity [*Collier et al.*, 1998; *Ridley*, 2000]. The reconstruction of the discontinuity normal from the currently available satellite measurements is quite difficult and not always possible [*Song and Russell*, 1999]. The tilt of the discontinuity front may produce asymmetry in the reaction time between the dayside and nightside ionosphere. An additional cause of asymmetry may be the deviation of the magnetic dipole from the Z axis of the GSM coordinate system.

[48] We repeated our simulations with a number of different solar wind parameters, such as IMF strength and solar wind speed, and found that the ionospheric reconfiguration time depends noticeably on both the solar wind speed and the IMF strength. In contrast, the "bow shock to ionosphere" communication time is virtually independent of the IMF strength but still depends on the solar wind velocity. In our simulations we did not find any dependence on the values of ionospheric Hall and Pederson conductivities for

the case of uniform conductivity distribution. We did not investigate any effects arising from nonuniform distribution of conductivities. The bow shock to ionosphere communication times in our simulations were in the range of 300–400 s, and the reconfiguration e-folding times were in the range of 260–450 s. These values are well within observational constraints and are reasonably consistent with the earlier MHD investigations of similar problems. We have also compared our modeling results to those of *Maynard et al.* [2001] for a similar set of parameters. While most important conclusions of the two models agree, there are several discrepancies, concerning for example the shape of the difference patterns for the ionospheric potentials and field-aligned currents. More work will be required to unambiguously assess the reasons for these disagreements.

[49] Using a 3-D time-dependent MHD model as a tool we have obtained ionosphere reconfiguration times consistent with available experimental observations. We consider this to be a contribution to the existing problem of model validation and an indication that MHD models are approaching the state when they can be routinely used for interpretation of data provided by ground-based and spaceborne instruments.

[50] **Acknowledgments.** We would like to thank Gordon Rostoker for his interest in this work and many stimulating discussions. K. K., R. R., and R. M. were supported in part by the Natural Sciences and Engineering Research Council of Canada and by the Canadian Space Agency. The Michigan group was supported by the NSF KDI grant ATM-9980078, NASA grant NAG 510504, and by DoD MURI grant F49620-01-1-0359. We also acknowledge the use of MACI computational resources, funded in part by Canada Foundation for Innovation, Alberta Innovation and Science Research Investment program, and the Universities of Alberta and Calgary.

[51] Arthur Richmond thanks J. M. Ruohoniemi and another reviewer for their assistance in evaluating this paper.

References

Amm, O., Comment on "A three-dimensional, iterative, mapping procedure for the implementation of an ionosphere-magnetosphere anisotropic Ohm's law boundary condition in global magnetohydrodynamic simulations" by Michael Goodman, *Ann. Geophys.*, *14*, 773–774, 1996.

Bargatze, L. F., D. N. Baker, R. L. McPherron, and E. W. Hones, Magnetospheric impulse response to many levels of geomagnetic activity, *J. Geophys. Res.*, *90*, 6387–6394, 1985.

Clauer, C. R., and E. Friis-Christensen, High-latitude dayside electric field and currents during strong northward interplanetary magnetic field: Observations and model calculations, *J. Geophys. Res.*, *93*, 2749–2757, 1988.

Collier, M. R., J. A. Slavin, R. P. Lepping, A. Szabo, and K. Ogilvie, Timing accuracy for the simple planar propagation of magnetic field structures in the solar wind, *Geophys. Res. Lett.*, *25*, 2509–2512, 1998.

Cowley, S. W. H., Magnetospheric asymmetries associated with the Y-component of the IMF, *Planet. Space Sci.*, *29*, 79–96, 1981.

DeZeeuw, D. L., T. I. Gombosi, C. P. T. Groth, K. G. Powell, and Q. F. Stout, An adaptive MHD method for global space weather simulations, *IEEE Trans. Plasma Sci.*, *28*, 1956–1965, 2000.

Dudeney, J. R., A. S. Rodger, M. P. Freeman, J. Pickett, J. Scudder, G. Sofko, and M. Lester, The nightside ionospheric response to IMF B_y changes, *Geophys. Res. Lett.*, *25*, 2601–2604, 1998.

Friis-Christensen, E., Y. Kamide, A. D. Richmond, and S. Matsushita, Interplanetary magnetic field control of high-latitude electric fields and currents determined from Greenland magnetometer chain, *J. Geophys. Res.*, *90*, 1325–1338, 1985.

Gombosi, T. I., D. L. DeZeeuw, C. P. T. Groth, and K. G. Powell, Magnetospheric configuration for Parker-spiral IMF conditions: Results of a 3D MHD simulation, *Adv. Space Res.*, *26*, 139–149, 2000a.

Gombosi, T. I., K. G. Powell, and B. vanLeer, Comment on "Modeling the magnetosphere for northward interplanetary magnetic field: Effects of electrical resistivity" by Joachim Raeder, *J. Geophys. Res.*, *105*, 13,141–13,147, 2000b.

Gombosi, T. I., G. Tóth, D. L. DeZeeuw, K. C. Hansen, K. Kabin, and K. G. Powell, Semirelativistic magnetohydrodynamcs and physics-based convergence acceleration, *J. Comput. Phys.*, *177*, 176–205, 2002.

Goodman, M. L., A three-dimensional, iterative, mapping procedure for the implementation of an ionosphere-magnetosphere anisotropic Ohm's law boundary condition in global magnetohydrodynamic simulations, *Ann. Geophys.*, *13*, 843–853, 1995.

Hairston, M. R., and R. A. Heelis, Response time of the polar ionospheric convection pattern to changes in the north-south direction of the IMF, *Geophys. Res. Lett.*, *22*, 631–634, 1995.

Khan, H., and S. W. H. Cowley, Observations of the response time of high-latitude ionospheric convection to variations in the interplanetary magnetic field using EISCAT and IMP-8 data, *Ann. Geophys.*, *17*, 1306–1335, 1999.

Landau, L. D., and E. M. Lifshitz, *Electrodynamics of Continuous Media*, Pergamon, New York, 1984.

Lockwood, M., and S. W. H. Cowley, Comment on "A statistical study of the ionospheric convection response to changing interplanetary magnetic field conditions using the assimilative mapping of ionospheric electrodynamics technique" by A. J. Ridley et al., *J. Geophys. Res.*, *104*, 4387–4391, 1999.

Lu, G., S. W. H. Cowley, S. E. Milan, D. G. Sibeck, R. A. Greenwald, and T. Moretto, Solar wind effects on ionospheric convection: A review, *J. Atmos. Sol. Terr. Phys.*, *64*, 145–157, 2002.

Maynard, N. C., et al., Response of ionospheric convection to changes in the interplanetary magnetic field: Lessons from a MHD simulation, *J. Geophys. Res.*, *106*, 21,429–21,451, 2001.

Murr, D. L., and W. J. Hughes, Reconfiguration timescales of ionospheric convection, *Geophys. Res. Lett.*, *28*, 2145–2148, 2001.

Papitashvili, V. O., B. A. Belov, D. S. Faermark, S. A. Golyshev, L. Gromova, and A. E. Levitin, Electric potential patterns in the northern and southern polar regions parameterized by the interplanetary magnetic field, *J. Geophys. Res.*, *99*, 13,251–13,262, 1994.

Powell, K. G., P. L. Roe, T. J. Linde, T. I. Gombosi, and D. L. DeZeeuw, A solution-adaptive upwind scheme for ideal magnetohydrodynamics, *J. Comput. Phys.*, *154*, 284–309, 1999.

Ridley, A. J., Estimation of the uncertainty in timing the relationship between magnetospheric and solar wind processes, *J. Atmos. Sol. Terr. Phys.*, *62*, 757–771, 2000.

Ridley, A. J., and C. R. Clauer, Characterization of the dynamic variations of the dayside high-latitude ionospheric convection reversal boundary and relation to interplanetary magnetic field orientation, *J. Geophys. Res.*, *101*, 10,919–10,938, 1996.

Ridley, A. J., G. Lu, C. R. Clauer, and V. O. Papitashvili, A statistical study of the ionospheric convection response to changing interplanetary magnetic field conditions using the assimilative mapping of ionospheric electrodynamics technique, *J. Geophys. Res.*, *103*, 4023–4039, 1998.

Ridley, A. J., G. Lu, C. R. Clauer, and V. O. Papitashvili, Reply, *J. Geophys. Res.*, *104*, 4393–4396, 1999.

Ridley, A. J., G. Crowley, and C. Freitas, An empirical model of the ionospheric electric potential, *Geophys. Res. Lett.*, *27*, 3675–3678, 2000.

Ridley, A. J., D. L. DeZeeuw, T. I. Gombosi, and K. G. Powell, Using steady-state MHD results to predict the global state of the magnetosphere-ionosphere system, *J. Geophys. Res.*, *106*, 30,067–30,076, 2001.

Ridley, A. J., K. C. Hansen, G. Tóth, D. L. DeZeeuw, T. I. Gombosi, and K. G. Powell, University of Michigan MHD results of the GGCM metrics challenge, *J. Geophys. Res.*, *107*(A10), 1290, doi:10.1029/2001JA000253, 2002.

Rostoker, G., D. Savoie, and T. D. Phan, Response of magnetosphere-ionosphere current systems to changes in the interplanetary magnetic field, *J. Geophys. Res.*, *93*, 8633–8641, 1988.

Ruohoniemi, J. M., and R. A. Greenwald, Statistical patterns of the high-latitude convections obtained from Goose Bay HF radar observations, *J. Geophys. Res.*, *101*, 21,743–21,763, 1996.

Ruohoniemi, J. M., and R. A. Greenwald, The response of high-latitude convection to a sudden southward IMF turning, *Geophys. Res. Lett.*, *25*, 2913–2916, 1998.

Ruohoniemi, J. M., S. G. Shepherd, and R. A. Greenwald, The response of high-latitude ionosphere to IMF variations, *J. Atmos. Sol. Terr. Phys.*, *64*, 159–171, 2002.

Saunders, M. A., M. P. Freeman, D. J. Southwood, S. W. H. Cowley, M. Lockwood, J. C. Samson, C. J. Farrugia, and T. J. Hughes, Dayside ionospheric convection changes in response to long-period interplanetary magnetic field oscillations: Determination of the ionospheric phase velocity, *J. Geophys. Res.*, *97*, 19,373–19,380, 1992.

Shepherd, S. G., R. A. Greenwald, and J. M. Ruohoniemi, A possible explanation for rapid, larger-scale ionospheric responses to southward turnings of the IMF, *Geophys. Res. Lett.*, *26*, 3197–3200, 1999.

Slinker, S. P., J. A. Fedder, W. J. Hughes, and J. G. Lyon, Response of the ionosphere to a density pulse in the solar wind: Simulation of traveling convection vortices, *Geophys. Res. Lett.*, *26*, 3549–3552, 1999.

Slinker, S. P., J. A. Fedder, J. M. Ruohoniemi, and J. G. Lyon, Global MHD simulation of the magnetosphere for November 24, 1996, *J. Geophys. Res.*, *106*, 361–380, 2001.

Song, P., and C. T. Russell, Time series data analyses in space physics, *Space Sci. Rev.*, *87*, 387–463, 1999.

Song, P., D. L. DeZeeuw, T. I. Gombosi, C. P. T. Groth, and K. G. Powell, A numerical study of solar wind-magnetosphere interaction for northward IMF, *J. Geophys. Res.*, *104*, 28,361–28,378, 1999.

Song, P., D. L. DeZeeuw, T. I. Gombosi, J. U. Kozyra, and K. G. Powell, Global MHD simulations for southward IMF: A pair of wings in the flanks, *Adv. Space Res.*, *28*, 1763–1771, 2001.

Tanaka, T., Interplanetary magnetic field B_y and auroral effects on high-latitude ionospheric convection patterns, *J. Geophys. Res.*, *106*, 24,505–24,516, 2001.

Todd, H., S. W. H. Cowley, M. Lockwood, D. M. Willis, and H. Lühr, Response time of the high-latitude dayside ionosphere to sudden changes in the north-south component of the IMF, *Planet. Space Sci.*, *36*, 1415–1428, 1988.

Valdivia, J. A., D. Vassiliadis, A. Klimas, and A. S. Sharma, Modeling the spatial structure of the high latitude magnetic perturbations and the related current systems, *Phys. Plasmas*, *6*, 4185–4194, 1999.

Weimer, D. R., Models of high-latitude electric potentials derived with a least error fit of spherical harmonic coefficients, *J. Geophys. Res.*, *100*, 19,595–19,607, 1995.

Weimer, D. R., A flexible, IMF dependent model of high-latitude electric potential having "space weather" applications, *Geophys. Res. Lett.*, *23*, 2549–2552, 1996.

Weimer, D. R., An improved model of ionospheric electric potentials including substorm perturbations and application to the Geospace Environment Modeling November 24, 1996, event, *J. Geophys. Res.*, *106*, 407–416, 2001.

C. R. Clauer, D. L. DeZeeuw, T. I. Gombosi, V. O. Papitashvili, and A. J. Ridley, Space Physics Research Laboratory, University of Michigan, Ann Arbor, MI 48109-2143, USA. (rclauer@umich.edu; darrens@engin.umich.edu; tamas@umich.edu; papita@umich.edu; ridley@umich.edu)

K. Kabin, R. Marchand, and R. Rankin, Department of Physics, University of Alberta, Edmonton, Alberta, Canada T6G 2J1. (kabin@phys.ualberta.ca; marchand@phys.ualberta.ca; rankin@space.ualberta.ca)